RSC Advances

PAPER

View Article Online
View Journal | View Issue

Cite this: *RSC Adv.*, 2017, **7**, 46336

Rapid self-healing and recycling of multiple-responsive mechanically enhanced epoxy resin/graphene nanocomposites

Chenting Cai,[a] Yue Zhang,[b] Xueting Zou,[a] Rongchun Zhang,[*c] Xiaoliang Wang,[b] Qiang Wu[a] and Pingchuan Sun[*ac]

The development of self-healing and recyclable crosslinked polymeric materials has drawn considerable attention in recent years. However, the bulk healing or remending speed is usually slow due to the high viscosity of high M_w polymers, and the low rate of thermal conduction from material surfaces into the central matrix. Herein, a rapid self-healing and recyclable high-performance crosslinked epoxy resin (ER)/graphene nanocomposite is reported by simultaneously incorporating thermally reversible Diels–Alder (DA) covalent bonds and multiple-responsive graphene into the ER matrix. Therefore, graphene in proximity to the DA crosslinkages can instantly trigger the retro-DA reactions by converting the absorbed energies (*e.g.* infrared light, microwave, *etc.*) into heat, and thus enables rapid self-healing and recycling. Furthermore, the well-dispersed graphene (<1 wt%) could significantly enhance the mechanical strength of the ER. *In situ* variable temperature solid-state NMR spectroscopy was used to monitor the reversible DA reactions at the molecular level, and the high healing and recycling efficiency of ER/graphene nanocomposites was well demonstrated by multiple approaches.

Received 21st August 2017
Accepted 23rd September 2017

DOI: 10.1039/c7ra09258j

rsc.li/rsc-advances

Introduction

In the past decades, synthetic polymeric materials have been widely used in a variety of fields including the transport industry, civil engineering, electronics, *etc.*, due to their exceptional physical and chemical properties. In particular, inspired by the biological healing function in nature, self-healing polymers have been the focus of recent studies on stimuli-responsive materials, due to their capability of repairing themselves after suffering damage or fracture.[1–11] Therefore, it is greatly beneficial for improving a material's service life, safety, sustainability and adaptability to a poor environment. Traditionally, microcapsules[8,12] or other microcontainers,[13] which store the repairing chemicals, are incorporated into the polymer matrix. However, in such systems, the chemical reactions can generally only take place once, and the mechanical properties of the materials may be severely deteriorated by the incorporation of microcontainers. While such conventional microcontainers can be replaced with 3D microvascular networks to enable repeatable healing,[14–16] the fabrication process is rather complex, and is not applicable to most materials. On the contrary, synthetic polymeric materials with intrinsic self-healing ability have achieved significant advances in recent years, where dynamic covalent bonds[2,17–20] or non-covalent supramolecular motifs[3,5,9,21,22] are incorporated into the molecular systems.[10,23] Generally, the healing of cracks involves four steps including approach of polymer chains, wetting, interdiffusion and re-entanglement.[24] Thus, the temperature for healing has to be above the glass transition temperature (T_g) to bestow the polymer chains enough mobility for the reconstruction of polymer network. As a result, the bulk healing/remending speed is usually slow because of the large viscosity of high M_w polymers and the low rate of thermal conduction from the fractured material surfaces into the centred polymer matrix. Therefore, it is quite essential to fabricate high performance polymeric materials with the capability of rapid self-healing and recycling. In addition, most self-healing materials can only be healed/recycled by a specific approach, which severely limits their applications in a wide range of circumstances. Furthermore, bestowing the materials with rapid self-healing and recycling capability will undoubtedly extend the service life of products, and thus reduce the energy consumption. Until now, it still remains a great challenge to develop crosslinked polymeric materials with excellent mechanical properties and superior capability of rapid self-healing, recycling and remolding *via* multiple approaches.

Because of their outstanding mechanical properties and multiple-responsiveness to infrared (IR) light and microwaves,

[a]*Key Laboratory of Functional Polymer Materials of Ministry of Education, College of Chemistry, Collaborative Innovation Center of Chemical Science and Engineering (Tianjin), Nankai University, Tianjin 300071, China. E-mail: spclbh@nankai.edu.cn*
[b]*Department of Polymer Science and Engineering, Nanjing University, Nanjing 210093, China*
[c]*State Key Laboratory of Medicinal Chemical Biology, Nankai University, Tianjin, 300071, P. R. China. E-mail: zrcrong@nankai.edu.cn*

graphene are widely utilized as fillers in fabricating mechanical enhanced nanocomposite materials.[6,25–29] Therefore, the combination of graphene and thermo-reversible covalent bonds, such as that formed by Diels–Alder (DA) reaction, provides an effective avenue to address the above mentioned challenge. Previously, graphene sheets were incorporated into linear commercial polyurethane to endow the material with enhanced mechanical properties as well as rapid self-healing *via* multiple approaches including heat, IR light and microwaves.[6] However, the incorporation of graphene sheets into thermo-reversible crosslinked polymer was rarely reported, not to mention the rapid self-healing capability of materials *via* multiple methods.[25] Herein, we report a novel thermo-reversible crosslinked epoxy resin (ER)/graphene nanocomposite, where the well-dispersed graphene sheets in proximity to the DA crosslinkages in the ER matrix can act as an intrinsic localized thermal source to trigger the retro-DA (rDA) reactions for healing by converting the absorbed external IR/microwave energies into heat. As a result, the incorporation of graphene not only improves the mechanical properties with respect to the pure ER matrix, but also remarkably enhances the efficiency of self-healing and recycling *via* multiple approaches as shown in Scheme 1. IR light, microwave and heat can all be used as external stimulus to trigger the rDA reactions for rapid self-healing and recycling. To our knowledge, this is the first example to achieve fast self-healing and recycling of DA-based crosslinked ER systems using microwave and IR irradiation.

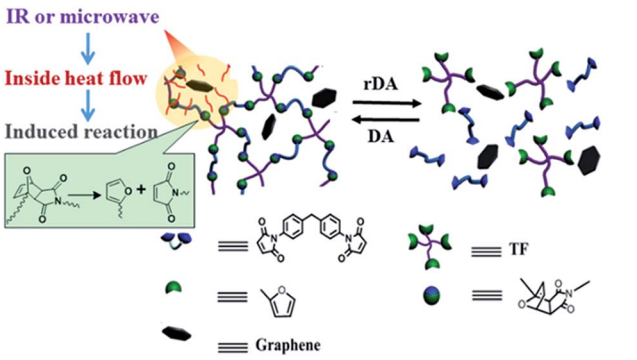

Scheme 1 Schematic diagram of the healing and recycling mechanism by triggering rDA reaction in thermo-reversible crosslinked polymers *via* multiple approaches including microwave, IR light, and heat.

Experimental

1. Sample preparation

1.1 Materials. Furfurylmercaptan (>99%) and triethylamine (Et_3N, >99%) were purchased from Sigma Aldrich (Shandong, China), while 1,1′-(methylenedi-4,1-phenylene) bismaleimide (BM, >96%) was obtained from TCI Chemicals Co., Ltd. (Tianjin, China). 4,4′-Methylenebis[*N*,*N*-diglycidylaniline] (>98%) and pentaerythritol glycidyl ether (>95%) was bought from Aladdin Chemistry Co., Ltd. (Shanghai, China) and Frontier Scientific. Inc. (Utah, USA), respectively. *N*-Methyl-2-pyrrolidone (NMP) and tetrahydrofuran (THF) was bought from Concord Technology Co. Ltd. (Tianjin, China). Graphene (0.4 mg ml^{-1}, dispersed in NMP solvent) was commercial available from Nanjing XFNANO Materials Tech Co., Ltd. All chemicals were used as received without any further treatment.

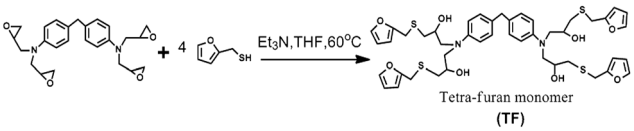

Scheme 2 Synthesis of TF.

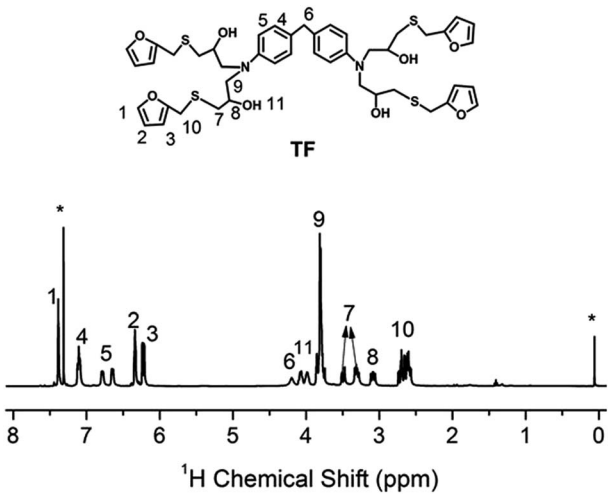

Fig. 1 ^1H NMR spectrum of TF in $CDCl_3$. "*" denotes the proton signals of chloroform (δ_{iso} = 7.26 ppm) and TMS (δ_{iso} = 0 ppm).

1.2 Synthesis of TF and TF-refer. The procedure for the synthesis of tetra-furan monomer (TF) was shown in Scheme 2. 4,4′-Methylenebis[*N*,*N*-diglycidylaniline] (44.2 g, 0.1 mol), furfurylmercaptan (45.6 g, 0.4 mol) and triethylamine (Et_3N, 0.4 g) were dissolved in 100 g THF solvent in a round bottom flask. Then, the mixture was stirred at 70 °C for 16 h. The final product (*i.e.* TF) was obtained by removing the THF solvent and Et_3N with reduced pressure distillation. The chemical structure of tetra-furan was confirmed by solution ^1H NMR spectroscopy, as shown in Fig. 1.

The procedure for the synthesis of TF-refer was shown in Scheme 3. Pentaerythritol glycidyl ether (36.0 g, 0.1 mol), furfurylmercaptan (45.6 g, 0.4 mol) and Et_3N (0.4 g) were mixed in a round bottom flask. The resulting mixture was stirred at 50 °C for 8 h. The final product (*i.e.* TF-refer) was obtained by removing Et_3N with reduced pressure distillation. The chemical structure of TF-refer was confirmed by ^1H NMR spectroscopy as shown in Fig. 2.

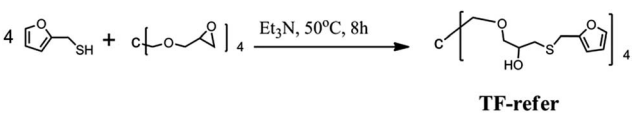

Scheme 3 Synthesis of TF-refer.

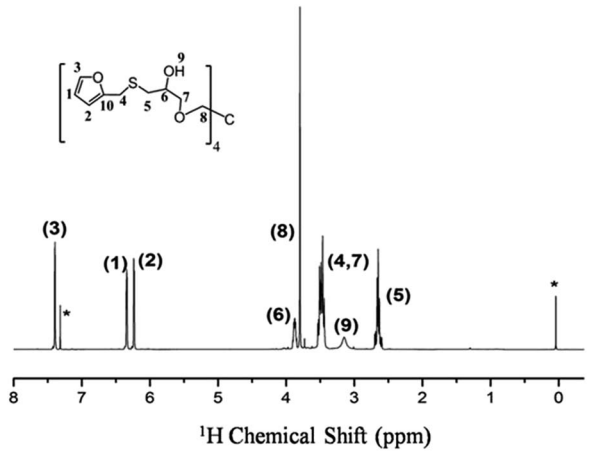

Fig. 2 ^{1}H NMR spectrum of TF-refer in $CDCl_3$. "*" denotes the proton signals of chloroform (δ_{iso} = 7.26 ppm) and TMS (δ_{iso} = 0 ppm).

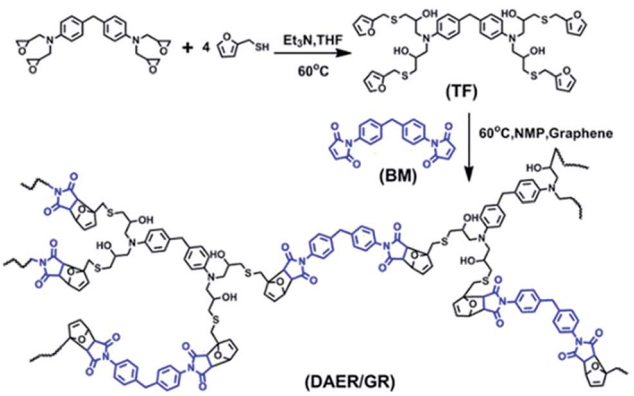

Scheme 4 Schematic synthetic route for thermo-reversible cross-linked ER/graphene nanocomposites.

1.3 Preparation of ER/graphene polymer nanocomposites. Preparation of ER/graphene polymer nanocomposites was shown in Scheme 4. Graphene was initially well dispersed in the NMP solvent. Then, BM and TF were added into the above solution to obtain a 30 wt% NMP solution. After ultrasonic treatment for 30 min, the resulting mixture was poured onto a Teflon mold, and cured at 60 °C for 12 h. The cured composite was dried at 65 °C in a vacuum oven for seven days. The final obtained samples were then cut into rectangle species for tensile measurement. Four samples, corresponding to a graphene weight fraction of 0, 0.25%, 0.5% and 0.75%, were prepared and named as DAER/GR, DAER/GR-0.25, DAER/GR-0.5, DAER/GR-0.75, respectively. The same procedures were followed for the preparation of DAER/GR-refer nanocomposites with a graphene weight fraction of 0.25%, using BM and TF-refer as the monomers for the crosslinking reactions.

2. Characterization

2.1 Mechanical testing. Stress–strain curves were measured on an UTM6103 mechanical testing instrument (Shenzhen Suns Technology Stock Co., LTD., China) in tensile mode at a room temperature of 20 °C. The samples were cut into a shape of 12 mm × 2 mm × 1 mm, and the strain rate is 5 mm min^{-1}.

2.2 Differential scanning calorimetry (DSC). DSC measurements were performed on a Mettler-Toledo DSC1 differential scanning calorimeter with a heating rate of 10 °C min^{-1} under nitrogen atmosphere. About 10 mg samples were encapsulated in 40 μL aluminum pans before measurements. TOPEM, a new stochastic temperature-modulated DSC technique introduced by Mettler-Toledo in late 2005,[30] was also perform to distinguish the glass transition process and rDA reaction of the polymeric materials. The temperature scan for TOPEM experiment was set from 0 °C to 150 °C to cover the glass transition and rDA reaction intervals. The underlying heating rate was set as 1 °C min^{-1}, and the amplitude of temperature pulse was set as 1 °C. The switching time range, which limits the duration of the pulses, was set as 15–30 s.

2.3 NMR experiments. Solution NMR experiments were performed on a Bruker AVANCE III NMR spectrometer with a proton resonance frequency of 400.13 MHz. The samples were dissolved in deuterated chloroform with a small amount of TMS as the internal reference standard.

High-field solid-state NMR experiments were performed on a Varian InfinityPlus-400 wide-bore (89 mm) NMR spectrometer operating at a ^{1}H frequency of 399.7 MHz and ^{13}C frequency of 100.5 MHz, respectively. A conventional 4 mm double-resonance HX CP/MAS NMR probe was used, and samples were placed in a 4 mm zirconia PENCIL rotor with a well-sealed cap and spacer. The magic angle spinning (MAS) was automatically controlled at 10 kHz within ±2 Hz with a magic angle spinning (MAS) speed controller. *In situ* variable-temperature CP-NOE experiments,[31] which are aimed to simultaneously enhance the signals of both rigid and mobile components, were carried out in the temperature range of 28–130 °C with a Varian Model-L950 temperature controller. Heteronuclear decoupling during the acquisition period was achieved by SPINAL-64 irradiation[32] with a radiofrequency strength of ~80 kHz. A temperature equilibration period of 10 min was implemented before NMR spectra were acquired. The recycle delay was set to 4 s.

Low-field solid-state NMR experiments were performed on a Bruker Minispec mq20 spectrometer at a 20 MHz proton resonance frequency. The sample temperature was controlled with a BVT3000 heater working with a flow of heated air. The Minispec has a typical π/2 pulse length of about 3.2 s, and a receiver dead time of about 13 s. Magic-sandwich echo (MSE)[33] pulse sequence was implemented to record the free induction decay (FID) signals, due to its capability of refocusing proton–proton dipolar couplings and thus to overcome the receiver dead time.

2.4 Fourier transform infrared spectroscopy. The infrared spectra were recorded with a resolution of 8 cm^{-1} and 16 scans per sample, using a Bio-Rad FTS6000 spectrometer and UMA600 microscope equipped with a Linkam FTIR600 heat stage.

2.5 Scanning electron microscopic (SEM). The field emission scanning electron microscopic (SEM) images were obtained on a JEOL-JSM 7500 microscope at 15 keV.

Results and discussion

The full procedure for the synthesis of ER/graphene nanocomposite is shown in Scheme 4, and the details can be found above in the Experimental section. All samples were dried at 65 °C in a vacuum oven for a week in order to completely remove the solvent. The formation of DA adducts is supported by the specific peaks at 3109 cm^{-1} in the FTIR spectra as will be discussed below. Typically, at the temperature above 110 °C, rDA reaction will be triggered such that the DAER and its nanocomposites will become liquids to allow rapid self-healing and recycling, whereas the DA reaction will dominate when the temperature decreases down to about 60–80 °C, leading to the re-formation of crosslinked network and recovery of mechanical properties.

The dispersion of graphene plays an important role in determining the final self-healing and recycling efficiency, and mechanical properties of the nanocomposites. Here, XRD and SEM experiments clearly indicate that the graphene sheets are well dispersed in ER matrix, as shown in Fig. 3. The well dispersed graphene layers can be clearly seen in the SEM image of DAER/GR-0.5 (Fig. 3b), in comparison to that of DAER (Fig. 3a). Besides, the sharp peaks corresponding to the pristine graphene completely disappear in the XRD spectrum of DAER/GR-0.5 (Fig. 3c). Both results clearly indicate that the graphene sheets are well dispersed and exfoliated in the ER matrix. Fig. 3d shows our proposed schematic view of graphene exfoliation assisted by the TF. In fact, for the small molecule TF, the two aromatic rings generally are not on the same conjugated plane due to the steric hindrances. When one of the aromatic rings on TF is in contact with graphene (mostly due to π–π interactions),

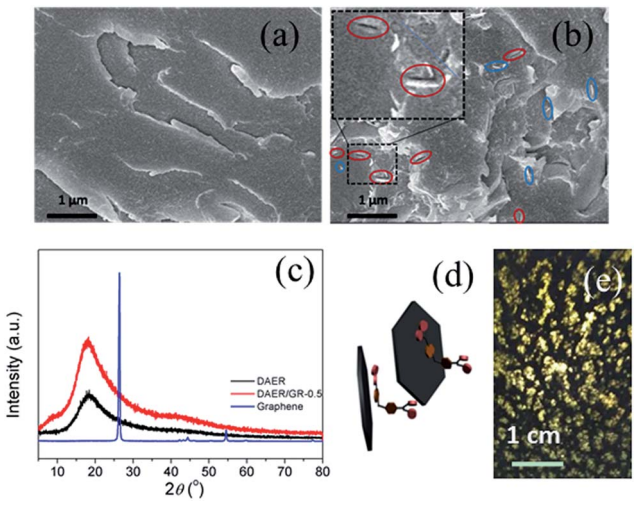

Fig. 3 SEM images of the cryogenically fractured surfaces of (a) DAER and (b) DAER/GR-0.5 samples. In DAER/GR-0.5 SEM image, the large hole defects indicated by the blue circles are ascribed to the separation of graphene from another fractured surface, while the red circles indicate the up straight graphene layers. (c) XRD curves for the pristine (without exfoliation) graphene, DAER, and DAER/GR-0.5 samples. (d) Schematic view of graphene exfoliation assisted by the TF. (e) The visual image of the DAER/GR-ref sample (with 0.5 wt% graphene) prepared using TF-refer monomers instead of TF.

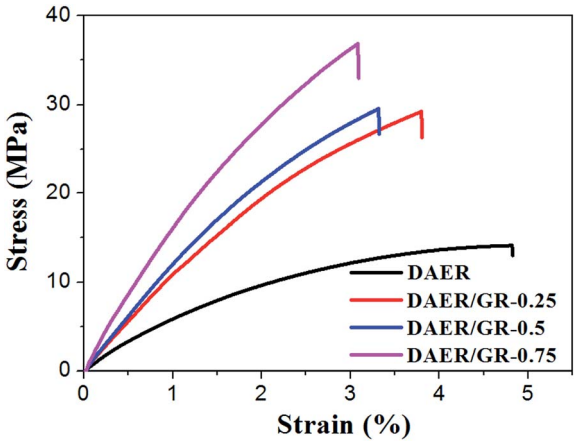

Fig. 4 Stress–strain curves of DAER and its nanocomposites measured with a strain rate of 5 mm min^{-1} at room temperature.

another aromatic ring on the TF will cause stronger steric hindrances for another graphene sheet to get close, and thus result in stable dispersion of graphene in the ER matrix. Instead, if the TF is replaced with TF-refer sample (Scheme 2), obvious aggregation of graphene can be observed from the visual image shown in Fig. 3e. Due to the well-dispersed graphene sheets in the crosslinked ER matrix, it was found that the incorporation of less than 1 wt% graphene did significantly enhance the Young's modulus and the tensile strength at break of the crosslinked ER materials as shown in Fig. 4 and Table 1. Besides, the elongation at break was not compromised severely. Furthermore, due to the incorporation of such small fraction of graphene, multiple approaches could be applied to re-heal, re-mold and recycle the materials as will be discussed in detail below.

The thermal self-healing and recycling behaviours of ER nanocomposites are closely related with the temperature dependent behaviours of DA and rDA reactions, which can be examined by the repeated DSC cycles and *in situ* variable temperature solid-state ^{13}C NMR spectroscopy. As is clearly shown in Fig. 5a, an overlapping between the glass transition and endothermic/exothermic transition at about 100–140 °C is observed during the successive heating/cooling cycles. Indeed, temperature modulated DSC experiment could be used to distinguish these two overlapped thermal transitions as shown in Fig. 5b, where the measured T_g is around 100 °C. It is worth noting that the measured T_g does not represent the actual glass

Table 1 Tensile properties of the DAER nanocomposites with variable graphene content

Samples	Tensile strength (MPa)	Young's modules (MPa)	Elongation at break (%)
DAER	14.1 + 1.1	511 + 50	5.1 + 0.3
DAER/GR-0.25	29.2 + 2.8	1073 + 30	3.9 + 0.1
DAER/GR-0.5	29.5 + 2.6	1195 + 28	3.4 + 0.1
DAER/GR-0.75	36.8 + 3.9	1546 + 19	3.1 + 0.2

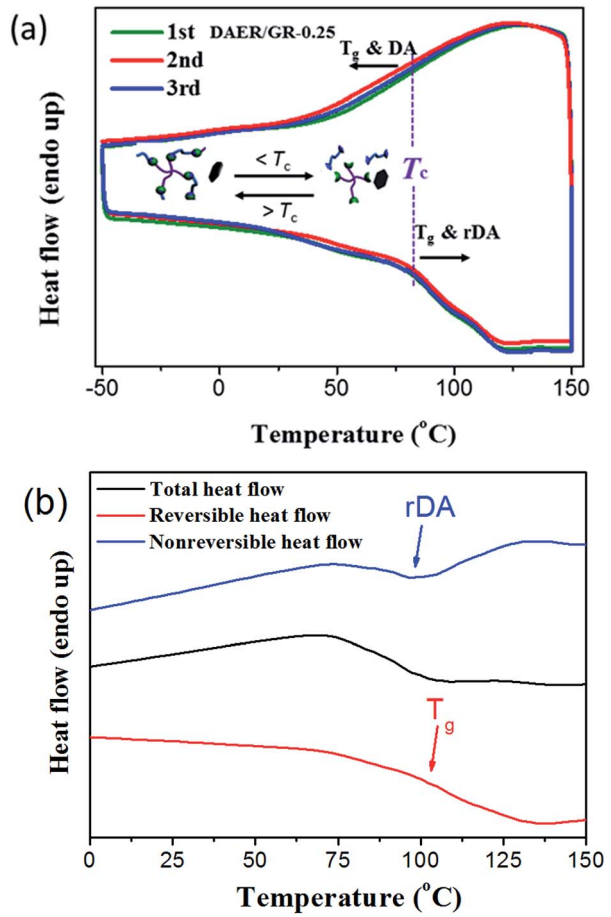

Fig. 5 (a) DSC traces of DAER/GR-0.5 in repeated cooling and heating cycles at a rate of 10 °C min^{-1}. (b) TOPEM curves of DAER/GR-0.5 sample. The heat flow for the reversible and nonreversible thermal transitions, corresponding to the glass transition and rDA reaction, are well separated, respectively. Thus, the glass transition temperature and the rDA temperature could be easily determined.

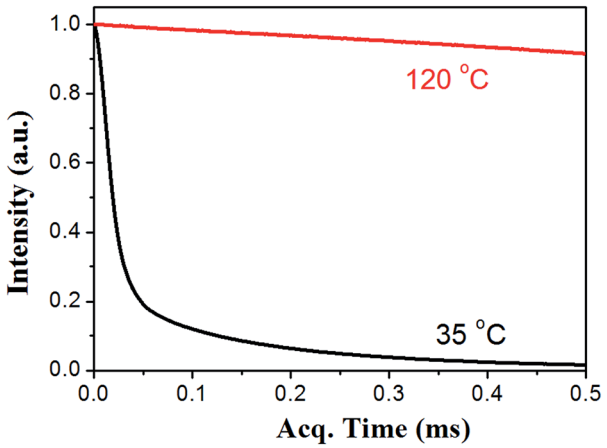

Fig. 6 The MSE-FID signals of DAER/GR-0.5 sample recorded at a temperature of 35 °C and 120 °C, respectively. At the low temperature, the sample is quite rigid, resulting in fast proton signal decay within tens of microsecond. In contrast, at a high temperature, the ER network is disassociated, and the sample becomes liquid, leading to extremely slow signal decay.

transition temperature of the original ER network. Instead, the measured T_g indicates the glass transition of partially dissociated ER network due to the rDA reactions. In the successive heating/cooling cycles, an excellent repeatability of the DSC traces is clearly observed in Fig. 5a, indicating the complete reconstruction of DA network within a short time scale during the DSC measurements with a heating rate of 10 °C min. Actually, most previously reported DA polymers have a slower DA kinetics as well as large deviation of the DSC traces in repeated thermal cycles.[17,19] Such difference is ascribed to the low viscosity and high mobility of small monomers for the ER network in comparison to the polymer chains for DA cross-linking, which can be further confirmed by the ^{1}H NMR experiments as shown in Fig. 6. At a temperature of 120 °C, the ^{1}H free-induction-decay (FID) signals show a liquid-like behaviour within an acquisition time of 0.5 ms, whereas generally obvious FID signal decay should be observed for the polymers at a temperature around T_g.[34] In order to further examine the DA and rDA reactions at the molecular level, variable temperature (VT) solid-state NMR experiments were performed to *in situ* detect the DA/rDA reactions, as shown in Fig. 7. Novel ^{13}C CP-NOE experiment recently developed in our group,[31] combing the merits of cross polarization (CP) and nuclear Overhauser (NOE) transfer, was implemented to record ^{13}C spectra, where all the ^{13}C signals were enhanced by proton-based polarization transfer.

As shown in Fig. 7, when the sample temperature was increased from 28 °C to 130 °C, it is clearly shown that two peaks at 82 and 91 ppm disappear; meanwhile, the intensities of peaks at 110, 143, and 152 ppm grow significantly. These results unambiguously indicate the presence of unreacted furan moieties in the system due to the dissociation of DA adducts at the high temperature. When the sample was cooled down to

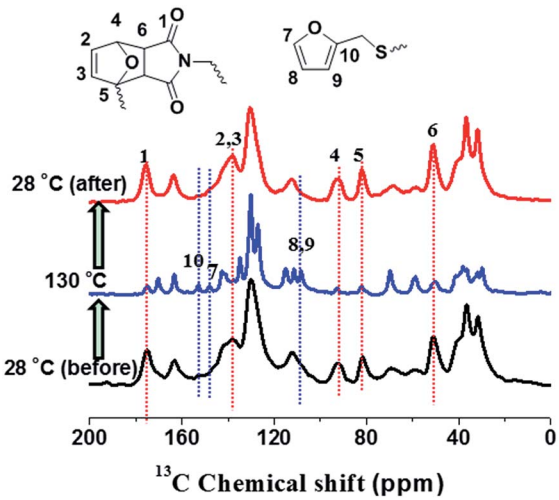

Fig. 7 *In situ* variable temperature solid-state ^{13}C NMR spectra of DAER at a thermal cycle of 28 °C (black), 130 °C (bule) and 28 °C (red), respectively. The CPNOE experiment was performed to record these spectra at a NOE mixing time of 0.5 s under a MAS rate of 10 kHz.

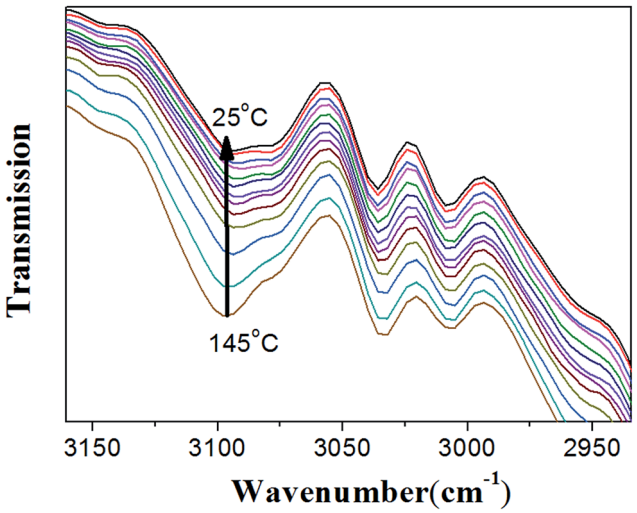

Fig. 8 *In situ* variable temperature FTIR spectra of DAER/GR-0.5 sample in the temperature range of 25–145 °C. The peaks at 3096 cm^{-1}, corresponding to the signal of C=C group in the BM monomer, can be considered as the characteristic peak for the DA reactions. With decreasing the temperature from 145 °C to 25 °C, the peak intensity of 3096 cm^{-1} gradually decreased, indicating the occurrence of progressive DA reaction.

28 °C, the ^{13}C spectrum is identical to that obtained before heating, demonstrating the complete reconstruction of DA crosslinked network. Therefore, *in situ* VT solid-state NMR experiments strongly confirmed the reversible cross-linking and the excellent recyclability in the DAER system. Alternatively, due to the presence of large fraction of DA adducts in the molecular systems, VT FTIR experiments results as shown in Fig. 8 could also provide evidences of the reversible DA crosslinking. The peak at 3096 cm^{-1}, corresponding to signal of C=C groups in the BM monomer, can be considered as the characteristic peak for the DA reactions. With decreasing the temperature, the intensity of the peak at 3096 cm^{-1} gradually decreased, demonstrating the occurrence of ongoing DA reactions. Because the IR light and microwaves can rapidly heat up the ER/graphene nanocomposites, the above VT solid-state ^{13}C NMR and FTIR results can also indirectly confirmed the reversible DA reactions in the nanocomposites under IR and microwave irradiation.

Since graphene can absorb IR light and electromagnetic wave efficiently and convert them into heat, it can also act as a localized thermal source to trigger the rDA reaction and thus enables rapid disassociation of the surrounding DA cross-linkages. As such, multiple approaches, including microwave and IR lights, can be used to re-mend the ER materials in addition to the conventional reprocessing method *via* high temperature molding or solution casting, as shown in Fig. 9. The DAER/GR-0.5 sample with thickness of 1 mm was firstly cut into tiny granules and put on a glass plate before re-mending. The microwave re-mending was achieved by keeping the sample in a 800 W domestic microwave oven operating at 2.45 GHz for a couple of minutes, while the re-mending by IR lights was achieved by keeping the sample under a 800 W IR lamp for

Fig. 9 Demonstration of the recyclability of DAER/GR-0.5 sample *via* multiple approaches, including microwave, heat and IR lights. The cracked tiny granule were put on a glass plate, and then irradiated with microwave, IR or heating without any other further manipulation.

four minutes. Similarly, simply increasing the sample temperature can also lead to the remending of the cracked pieces. As can be clearly seen in Fig. 9, all the re-mended samples have become integrated ones instead of separated granules. The healing and remending was quite easy and straightforward, since no external manipulation was employed during heating and IR/microwave irradiation periods. It is expected that more complex remolding can be achieved easily during heating or IR/microwave irradiation periods, such as shaping, 3D printing, and so on. In fact, the intrinsic mechanism of the healing is due to the reconstruction of DA crosslinking network by the disassociation and re-association of DA adducts *via* rDA and DA reaction, respectively. Graphene can efficiently convert microwave and IR energies into heat, and thus enable the fast occurrence of rDA reactions. The mechanical properties of the recycled polymers with different graphene content were further examined by tensile tests, as shown in Fig. 10, which well indicated the excellent thermally recyclability of the DAER/GR nanocomposites.

Due to the multi-responsive nature of DAER/GR materials, it is also possible to achieve targeted healing by adapting

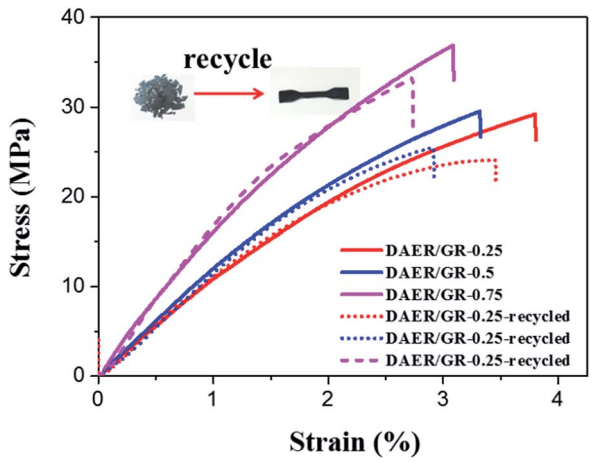

Fig. 10 Comparison of the stress–strain curves for the as-synthesized and recycled DAER/GR samples. It is clearly shown that the mechanical properties of the recycled sample is nearly identical to the as-synthesized ones, demonstrating the excellent thermally recyclability.

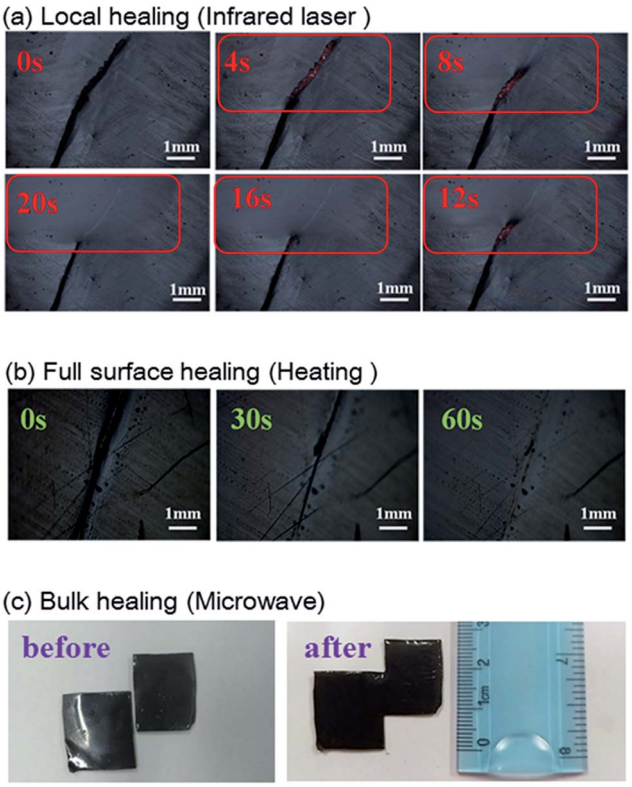

Fig. 11 Optical microscopy images of the selective healing enabled by multiple approaches, including (a) IR laser for local crack healing, (b) heating for full surface healing, and (c) microwave for bulk material healing. The ruler is used to indicate the size of the sample for bulk healing.

appropriate approaches, as shown in Fig. 11. A selective localized healing, noted by red rectangle in Fig. 11a, can be achieved by an IR laser, while the healing of a large crack on the surface can be achieved by simple thermal heating (Fig. 11b). In fact, only the temperature of the local place irradiated by IR laser will be affected as shown in Fig. 12a and b. Thus, the local healing can be achieved rapidly without affecting the integrity of the whole sample. Fig. 12c shows the sample temperature as a function of the IR laser irradiation time for DAER/GR nanocomposites with different graphene content. As is clearly shown, the local temperature of the place irradiated by IR laser increased very fast with increasing graphene content. For the healing of two bulk samples, it is only required to attach the two cut samples together and keep the sample in the microwave oven for a short time (Fig. 11c). It is worth noting that all the healing could be achieved in only a few minutes, or even seconds depending on the cracks. Such rapid and efficient healing can be ascribed to the fast disassociation of the DA network induced by the local heat from graphene absorbing IR lights/microwaves as well as the low viscosity of the ER monomer for DA reactions. Therefore, such molecular system is technically similar to the supramolecules assembled from the small molecular *via* non-covalent interactions. However, the presence of covalent Diels–Alder bonds will render the materials with superior mechanical properties to the supramolecules

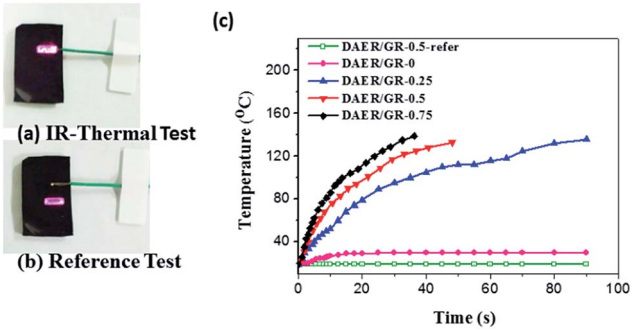

Fig. 12 Experiments for measuring the sample temperature increase induced by the IR laser irradiation. (a) Experimental setup for measuring the temperature on the place where the IR laser is irradiated. (b) Experimental setup for temperature measurement on the sample surface where the IR laser is not irradiated. (c) The sample temperature as a function of the IR laser irradiation time for DAER/GR nanocomposites with different graphene content.

assembled *via* non-covalent interactions. Without doubt, such rapid healing efficiency will greatly benefit extending the service life of materials as well as the recycling of products.

Conclusions

A novel mechanical enhanced self-healing ER/graphene nanocomposite is reported. It is found that 0.5 wt% graphene could significantly enhance the strength of crosslinked ER matrix by more than two times. In addition, ER/graphene nanocomposites can be rapidly and efficiently healed *via* multiple approaches, including heat, IR light, and microwave, due to the multiple responsive nature of graphene. In fact, the graphene in proximity to the DA crosslinkages in ER matrix can act as an intrinsic localized thermal source to trigger the rDA reactions for healing/recycling by converting the absorbed external energies into heat. As such, depending on the healing requirements, such as specific localized healing, full surface crack healing, or bulk sample re-mending, appropriate approaches can be chosen for rapid and efficient healing. These experimental findings here, together with the widespread uses of the ER materials in the industry and daily life, indicate that the ER/graphene nanocomposite could act as a promising self-healing material and find wide applications in various fields. Overall, the outcomes here could provide guidance for the design and fabrication of high-performance polymeric materials with rapid self-healing, recyclability and multiple-responsibility.

Conflicts of interest

There are no conflicts to declare.

Acknowledgements

The authors are grateful for the financial support by the National Natural Science Foundation of China (NSFC) through the General Programs. (No. 21534005 and 21374051), China

postdoctoral Science Foundation (No. 2016M601249), PCSIRT (IRT1257) and the 111 Project (B12015).

Notes and references

1 M. A. C. Stuart, W. T. S. Huck, J. Genzer, M. Muller, C. Ober, M. Stamm, G. B. Sukhorukov, I. Szleifer, V. V. Tsukruk, M. Urban, F. Winnik, S. Zauscher, I. Luzinov and S. Minko, *Nat. Mater.*, 2010, **9**, 101.
2 X. Chen, M. A. Dam, K. Ono, A. Mal, H. Shen, S. R. Nutt, K. Sheran and F. Wudl, *Science*, 2002, **295**, 1698.
3 P. Cordier, F. Tournilhac, C. Soulie-Ziakovic and L. Leibler, *Nature*, 2008, **451**, 977.
4 D. W. R. Balkenende, C. A. Monnier, G. L. Fiore and C. Weder, *Nat. Commun.*, 2016, **7**, 10995.
5 C.-H. Li, C. Wang, C. Keplinger, J.-L. Zuo, L. Jin, Y. Sun, P. Zheng, Y. Cao, F. Lissel, C. Linder, X.-Z. You and Z. Bao, *Nat. Chem.*, 2016, **8**, 618.
6 L. Huang, N. Yi, Y. Wu, Y. Zhang, Q. Zhang, Y. Huang, Y. Ma and Y. Chen, *Adv. Mater.*, 2013, **25**, 2224.
7 M. W. Urban, *Nat. Chem.*, 2012, **4**, 80.
8 S. R. White, N. R. Sottos, P. H. Geubelle, J. S. Moore, M. R. Kessler, S. R. Sriram, E. N. Brown and S. Viswanathan, *Nature*, 2001, **409**, 794.
9 Y. Chen, A. M. Kushner, G. A. Williams and Z. Guan, *Nat. Chem.*, 2012, **4**, 467.
10 Y. Yang and M. W. Urban, *Chem. Soc. Rev.*, 2013, **42**, 7446.
11 J. Hentschel, A. M. Kushner, J. Ziller and Z. Guan, *Angew. Chem.*, 2012, **124**, 10713.
12 K. Kratz, A. Narasimhan, R. Tangirala, S. Moon, R. Revanur, S. Kundu, H. S. Kim, A. J. Crosby, T. P. Russell, T. Emrick, G. Kolmakov and A. C. Balazs, *Nat. Nanotechnol.*, 2012, **7**, 87.
13 D. Y. Wu, S. Meure and D. Solomon, *Prog. Polym. Sci.*, 2008, **33**, 479.
14 K. S. Toohey, N. R. Sottos, J. A. Lewis, J. S. Moore and S. R. White, *Nat. Mater.*, 2007, **6**, 581.
15 C. J. Hansen, W. Wu, K. S. Toohey, N. R. Sottos, S. R. White and J. A. Lewis, *Adv. Mater.*, 2009, **21**, 4143.
16 D. Therriault, S. R. White and J. A. Lewis, *Nat. Mater.*, 2003, **2**, 265.
17 S. Yu, R. Zhang, Q. Wu, T. Chen and P. Sun, *Adv. Mater.*, 2013, **25**, 4912.
18 G. Deng, C. M. Tang, F. Y. Li, H. F. Jiang and Y. M. Chen, *Macromolecules*, 2010, **43**, 1191–1194.
19 S. Chen, F. Wang, Y. Peng, T. Chen, Q. Wu and P. Sun, *Macromol. Rapid Commun.*, 2015, **36**, 1687.
20 K. Imato, M. Nishihara, T. Kanehara, Y. Amamoto, A. Takahara and H. Otsuka, *Angew. Chem., Int. Ed.*, 2012, **51**, 1138.
21 C. Koopmans and H. Ritter, *Macromolecules*, 2008, **41**, 7418–7422.
22 F. Herbst, D. Döhler, P. Michael and W. H. Binder, *Macromol. Rapid Commun.*, 2013, **34**, 203.
23 R. J. Wojtecki, M. A. Meador and S. J. Rowan, *Nat. Mater.*, 2011, **10**, 14.
24 Y. H. Kim and R. P. Wool, *Macromolecules*, 1983, **16**, 1115.
25 S. Wu, J. Li, G. Zhang, Y. Yao, G. Li, R. Sun and C. Wong, *ACS Appl. Mater. Interfaces*, 2017, **9**, 3040.
26 C. S. Boland, U. Khan, G. Ryan, S. Barwich, R. Charifou, A. Harvey, C. Backes, Z. Li, M. S. Ferreira, M. E. Möbius, R. J. Young and J. N. Coleman, *Science*, 2016, **354**, 1257.
27 M. Wang, X. Duan, Y. Xu and X. Duan, *ACS Nano*, 2016, **10**, 7231.
28 J. H. Li, G. P. Zhang, L. B. Deng, S. F. Zhao, Y. J. Gao, K. Jiang, R. Sun and C. P. Wong, *J. Mater. Chem. A*, 2014, **2**, 20642–20649.
29 H. Kim, A. A. Abdala and C. W. Macosko, *Macromolecules*, 2010, **43**, 6515.
30 J. E. K. Schawe, T. Hütter, C. Heitz, I. Alig and D. Lellinger, *Thermochim. Acta*, 2006, **446**, 147.
31 R. C. Zhang, K. H. Mroue and A. Ramamoorthy, *J. Magn. Reson.*, 2016, **266**, 59.
32 B. M. Fung, A. K. Khitrin and K. Ermolaev, *J. Magn. Reson.*, 2000, **142**, 97.
33 M. Mauri, Y. Thomann, H. Schneider and K. Saalwächter, *Solid State Nucl. Magn. Reson.*, 2008, **34**, 125.
34 R. Zhang, T. Yan, B.-D. Lechner, K. Schröter, Y. Liang, B. Li, F. Furtado, P. Sun and K. Saalwächter, *Macromolecules*, 2013, **46**, 1841.